Small

NANO · MICRO small
www.small-journal.com

RESEARCH ARTICLE

Interfacial Plating Driving Convection-Like Motion of a Sandwiched Nanocrystal

Yueqing Yang[1,2] | Degang Xie[1] | Shuhei Shinzato[3] | Zhiyu Nie[1] | Xinyao Wang[1] | Suyang Sun[4] | Wei Zhang[4] | Jingzhao Chen[5] | Hongjun Ye[5] | Jianyu Huang[5] | En Ma[4] | Shigenobu Ogata[3] | Ju Li[6] | Zhiwei Shan[1]

[1]Center for Advancing Materials Performance from the Nanoscale (CAMP-Nano), State Key Laboratory for Mechanical Behavior of Materials, Xi'an Jiaotong University, Xi'an, P. R. China | [2]State Grid Shandong Electric Power Research Institute, Jinan, P. R. China | [3]Department of Mechanical Science and Bioengineering, The University of Osaka, Osaka, Japan | [4]Center for Alloy Innovation and Design (CAID), State Key Laboratory for Mechanical Behavior of Materials, Xi'an Jiaotong University, Xi'an, P. R. China | [5]Clean Nano Energy Center, State Key Laboratory of Metastable Materials Science and Technology, Yanshan University, Qinhuangdao, P. R. China | [6]Department of Nuclear Science and Engineering and Department of Materials Science and Engineering, Massachusetts Institute of Technology, Cambridge, Massachusetts, USA

Correspondence: Degang Xie (dg_xie@xjtu.edu.cn) | Shigenobu Ogata (ogata@me.es.osaka-u.ac.jp) | Ju Li (liju@mit.edu) | Zhiwei Shan (zwshan@xjtu.edu.cn)

Received: 9 October 2025 | **Revised:** 22 April 2026 | **Accepted:** 28 April 2026

Keywords: back-stress | convection-like motion | nanocrystal | thermo-mechanical migration | ultra-high temperature gradient

ABSTRACT

In crystalline solids, thermally driven atomic fluxes are generally linked to surface reshaping or coarsening, not sustained translation of an intact crystal. We show that when nanoscale Cu, Ag, and Al crystals are confined between two plates and subjected to axial temperature gradients approaching 10^8 K m^{-1}, they sustain a persistent, convection-like bidirectional mass flow. Thermo-mechanical-induced surface migration transports atoms from the hot end to the cold end, where interfacial insertion generates a self-regulated compressive back stress of up to 10^2 MPa—sufficient to push the crystalline core in the reverse direction. This closed-loop transport, coupling directional surface diffusion with rigid-body motion, is supported by molecular dynamics simulations and theoretical analysis. The findings reveal a previously unrecognized regime of mass-stress coupling in solids, opening new routes for solid-based thermal actuation and informing the thermal-mechanical reliability of nanoscale devices.

1 | Introduction

A steep temperature gradient is one of the most powerful thermodynamic drivers for atomic transport, capable of biasing the motion of atoms and vacancies alike [1, 2]. In solids, however, its consequences are usually conceived in familiar terms: surfaces reshape, grains coarsen, and interfaces evolve. The decisive event is not simply that atoms migrate, but where they are ultimately accommodated. When they are deposited onto a free surface, the usual outcome is morphological relaxation through surface-diffusion-mediated reshaping, dewetting or coarsening of nanoscale structures [3–8]. When they are inserted into a confined interface, by contrast, the same atomic flux can instead build substantial internal stress, destabilize the solid mechanically, and potentially drive motion of the crystal itself [9, 10]. In bulk metals, such a thermally driven motion is rarely realized, because lattice rigidity resists displacement and the high thermal conductivity of metals suppresses the large gradients required to sustain substantial atomic fluxes. At the nanoscale, by contrast, both restrictions weaken sharply. Surfaces become dominant kinetic pathways, thermal transport becomes size-limited [11, 12], and a temperature difference of only a few kelvin across tens

Yueqing Yang and Degang Xie contributed equally to this work.

of nanometers can produce gradients approaching 10^8 K m^{-1} [1, 13], strong enough to generate extraordinary directional mass transport that renders the material to acquire a mode of liquid-like deformability.

This raises a basic but unresolved question: under extreme nanoscale thermal gradients, where do migrating atoms go? Our earlier work [1] showed that external loading can steer this choice: tension promotes atomic insertion into an interface, whereas shear redirects atoms toward free-surface overflow. Yet the preferred deposition pathway, in the absence of applied pulling or shearing, has remained unknown. Will atoms still be driven into a confined interface, or will they follow the energetically simpler path of free-surface deposition?

Here, we address this question by confining metallic nanocolumns between rigid plates and imposing ultra-high axial temperature gradients, but without applied pulling or shearing. This configuration provides a pure test of whether thermal driving and geometric confinement alone can dictate the deposition pathway—a choice that ultimately determines whether a nanosolid merely grows in place or engages in directed, collective motion. We show that atoms do not simply accumulate on free surfaces. Instead, they are preferentially inserted into the cold-side interface, where they generate a self-regulated compressive back stress large enough to drive reverse translation of the crystalline core. The result is a persistent convection-like circulation in a solid: directional surface transport from hot to cold, coupled to rigid-body motion in the opposite direction. This identifies a previously unrecognized mode of mass-stress coupling in crystalline solids and points to a new route for converting heat directly into mechanical actuation at the nanoscale, suggesting new opportunities for designing nanoscale actuators and engines.

2 | Results

2.1 | Convection-Like Motion in Crystalline Metallic Nanocrystals

Figure 1 and Video S1 present a representative case of convection-like motion in a crystalline copper column, 58–115 nm in length. In situ imaging reveals solid features emerging from the cold-side interface (tungsten/column) and translating toward the hot side. These features—whether external profile contours or internal diffraction contrast—remain essentially unchanged during their transit, preserving both shape and relative spacing. For example, the two band-like features M1 and M2 in Figure 1a–e move downward in unison, as evidenced by their increasing separation from the reference dash lines. Throughout this motion, the copper column retains distinct crystal facets and diffraction contrast, confirming its crystalline nature [14].

To quantify this motion, we tracked the apparent (equivalent) diameter d along the column height h over time using a pixel-based image processing method (Figure 1f). The resulting contour map consists of nearly parallel, same-colored stripes that slope from upper left to lower right—clear evidence that the crystalline core moves from cold to hot as a near-rigid body. The slope of each stripe yields the translation speed, which ranges from 19 to 78 nm s^{-1} depending on the column length and contact area (Figure S4, Note S3). A systematic "longer is slower" trend emerges, consistent with a reduced driving flux for longer columns.

At first glance, this motion against the temperature gradient appears anomalous. It resembles the continuous growth of the copper column from the tungsten tip, yet the tip contains no copper source. Pre-contact tests showed a clean, non-wetting tungsten surface (Figure S5), and DFT calculations confirmed the absence of bulk miscibility between W/WO_3 and Cu (Note S1 and Figure S6). EDX analysis verified that the column shares the same composition as the hot copper substrate (Figure S7). Moreover, when a segment of the downward-moving column reaches the hot end, it does not accumulate but instead disappears—often preceded by local necking, as indicated by the red arrow in Figure 1a–e and the blued zones in Figure 1f at ~5, 23, and 35 s. These observations indicate that atoms are continuously removed from the hot side, likely feeding growth at the cold interface. Together, they suggest a self-sustained, mass-conserving motion in which atoms circulate between the hot and cold ends, making it essential to resolve the detailed flow path of atomic transport within the column.

The in situ observations reveal a clear downward translation of the crystalline core, but the complementary upward pathway of atoms—how they travel from the hot end back to the cold end—remains to be identified. Our previous work [1] demonstrated that under similar conditions, a large atomic flux can migrate along the surface via thermomigration. Finite element modelling (Figure S8) indicates that the axial temperature gradient in the present copper columns can reach ~10^8 K m^{-1}. Such an extreme gradient drives surface transport through two coupled contributions: a direct thermomigration flux, $\boldsymbol{J}_{\mathbf{T}}$ ~1.81×10^{23} atoms m^{-2} s^{-1}, and a stress-gradient-assisted flux $\boldsymbol{J}_{\sigma}$ ~1.14×10^{23} atoms m^{-2} s^{-1}, arising from the concomitant thermal stress gradient $\nabla\sigma$ (Note S4). Together, these contributions establish a coupled thermo-mechanical surface transport pathway that rapidly conveys Cu atoms from the hot base to the cold interface. Importantly, neither the magnitude of this flux nor the observed mass circulation requires the presence of a fully developed disordered pre-melting shell. Existing studies instead suggest that structurally resolvable surface disorder emerges only under much more extreme thermal conditions. For example, in Sn nanoparticles, a distinct quasi-liquid overlayer was detected only above ~0.92 T_m, where it nucleated a few monolayers thick and thickened progressively into the core [15]. Such a crystal-core–liquid-shell metallic nanorod structure can sustain rapid superplasticity through a diffusion-mediated plasticity mechanism, where the outer "liquid-like" layer facilitates rapid surface diffusion, contributing to extraordinary super-elongation without necking [16]. By contrast, under sub-melting conditions, surface instability can remain confined to the outermost atomic layer while the underlying crystal remains structurally intact, as shown for Au(200) [17], and direct observations in Ag nanowires further demonstrate that highly active surface diffusion can already mediate pronounced deformation far below the melting point without any resolved disordered surface phase [18]. Our experiments were conducted at relatively modest homologous temperatures (~0.72 T_m for Al, ~0.50 T_m for Cu, and ~0.46 T_m for Ag), making a disordered pre-melting state less likely than in near T_m systems where quasi-liquid layers have been directly resolved [15]. In contrast, the active layer in our Cu, Ag, and Al

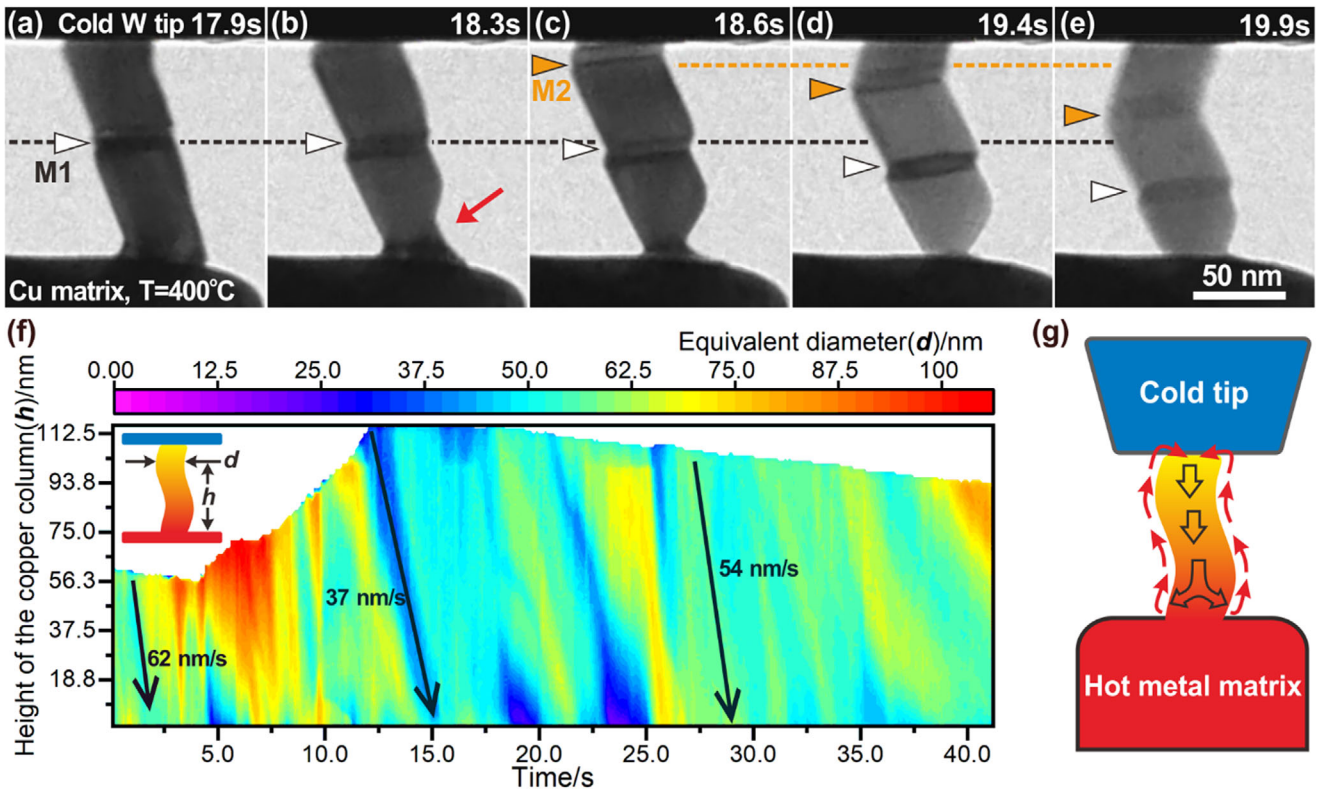

FIGURE 1 | A typical convective-like motion occurring in a crystalline copper nano-column. (a–e), Sequence images extracted from the recorded video (Movie S1) to show the movement of the nano-column. The time is labeled at the upper right corner. The red arrow in (b) indicates the shrinkage in diameter at the bottom. The column movement is indicated by the position change as referenced by the two twin-like markers (M1 and M2). The black and orange dashed horizontal lines represent the original positions for M1 at 17.9s and M2 at 19.4s, respectively. (f) The contour plot shows the change of equivalent diameter (d) at different height positions (h) as a function of time. The definitions of d and h are indicated in the inset at the upper-left corner. Black arrows represent the downward motion of certain features, with the moving speed labeled near the arrows. (g) The schematic illustration of the experimental setup, with a heated metal matrix as the hot end and a tungsten tip as the cold end. Red arrows indicate surface mass transport, while black hollow arrows show the movement of the column. Scale bar, 50 nm.

nano-columns is more likely to be one or two atomic layers, which remain predominantly crystalline with slightly dilated atomic spacing, rather than a fully disordered pre-melting layer. This interpretation naturally explains the simultaneous shrinkage at the hot end and growth at the cold end, thereby satisfying the mass balance required by the observed circulation.

Direct imaging of the upward atomic pathway is currently beyond the capability of our in situ TEM setup, as the transport is confined to an ultrathin surface layer and occurs on timescales shorter than the recording limit. The continuously changing column orientation, along with drift and vibration from the piezo-driven cold probe, further complicates stable atomic-resolution imaging of this dynamically evolving surface layer. We therefore infer the upward pathway from convergent indirect evidence. First, the circulation ceases once a surface oxide forms on Al columns (Note S2 and Figure S2), confirming both the presence of surface mass transport and its indispensable role in driving the circulation. Furthermore, the observed "longer is slower" trend naturally aligns with this mechanism, as lengthening the column directly reduces the axial temperature gradient and, consequently, the driving surface flux decreases (Note S3). We also evaluated the possible coexistence of other mass-transfer processes, including grain-boundary thermomigration, bulk thermomigration, evaporation/sublimation, accidental mass transfer, temperature-induced surface tension effect, electron-beam effects, and electrical effect, and found that they can either be excluded or considered minor contributions, with negligible influence on the observed convection-like motion (Note S4 and Figure S9).

In summary, a gigantic temperature gradient can induce a continuous, closed-loop mass flow in nanoscale single crystals of pure metal. The circulation follows a core–shell pattern: thermo-mechanical driven surface diffusion transports atoms from hot to cold along the outer layers, while the crystalline core translates in the opposite direction as a rigid body (Figure 1g). In materials science terminology, convection—or "displacive" motion—refers to the translation of the atomic center of mass within a reference volume, whereas diffusion involves additional random displacements beyond this translation [19]. Our observations thus constitute a previously unreported form of thermally driven circular convection-like motion in a solid. While analogous to Rayleigh–Bénard convection in that it is powered by a temperature gradient [20], the driving mechanism here is entirely different: no gravity or buoyancy is involved, only the directed thermo-mechanical migration of surface atoms. From the trajectory data (Figure S4), we estimate that a representative

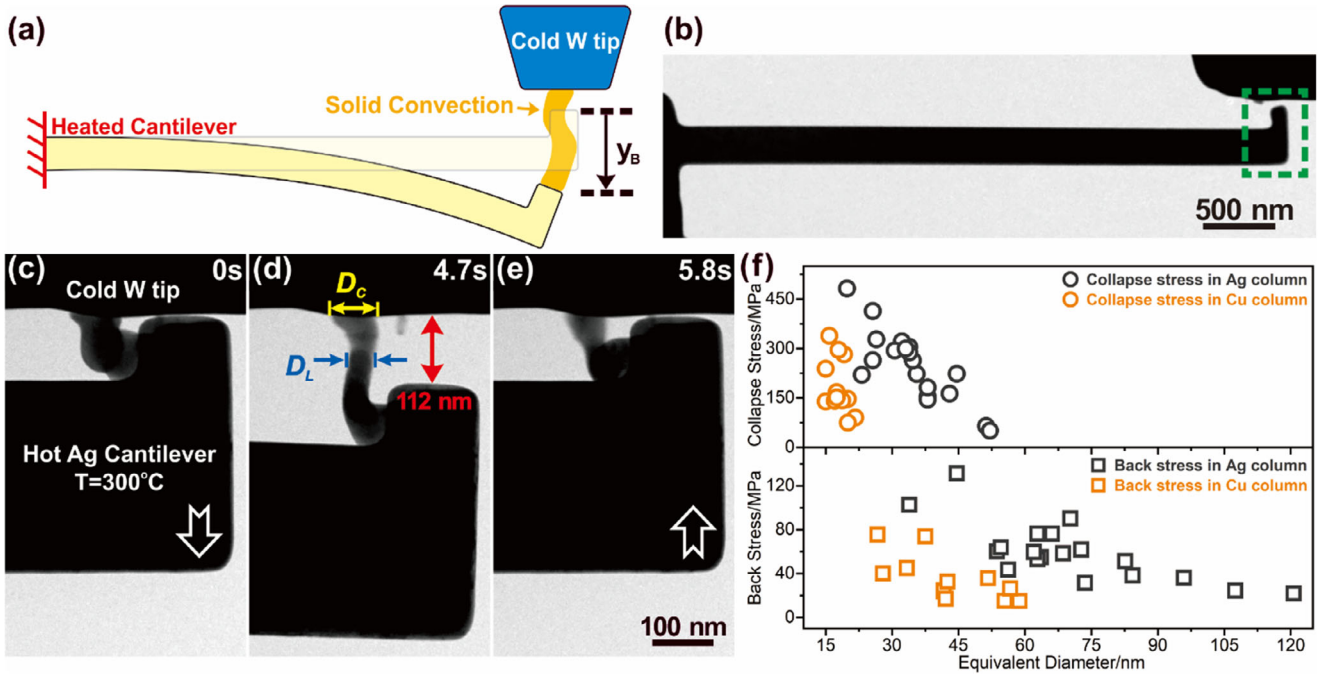

FIGURE 2 | Generation of back-stress at the cold side interface. (a,b) Schematic illustration and a real image of the experimental setup for quantitatively measuring the back-stress. The heated cantilever is an Ag or Cu cantilever. The green dash rectangle indicates the observed area. (c–e), Three snapshots from a typical bending cycle to show the shape evolution of an Ag nano-column and the change of cantilever positions. (c) is at the beginning of the bending cycle, and (d) shows the nano-column immediately before the collapse, accompanied by the maximum deflection of the cantilever within this cycle. The maximum deflection, equivalent contact diameter (D_C), and equivalent minimum diameter (D_L) were measured. (e) is after the collapse of the nano-column and spring-back of the cantilever. White arrows in (c,e) indicate the moving direction of the cantilever. (f), Plot of the measured contact back-stress and collapse back-stress versus equivalent diameter for silver and copper columns during the convection-like motion. Scale bars (b), 500 nm, (c,e), 100 nm.

volume element in the column can complete ~21 circulation cycles within 41.2 s.

2.2 | Measurement of the Back Stress at the Cold Interface

Coupled thermo-mechanical transport drains atoms from the hot end of the column, creating a tensile pull along its length. However, the rigid-body translation of the crystalline core also requires a compressive push from the opposite side. This driving force originates at the cold interface, where incoming atoms are inserted into the confined contact region, generating a diffusion-induced compressive stress—known as back stress [21–23]. In our experiments, columns occasionally buckled during motion (Figure S10), directly confirming the presence of such a compressive load. The mechanism is consistent with the asymmetric thermal response of the two ends: the hot base, with higher diffusivity, readily sends atoms toward the cold side, while the colder interface responds more sluggishly and in a more displacive fashion. As atoms accumulate preferentially near the contact perimeter, they exert a lateral "traffic jam" force that develops into a measurable back stress.

To quantify this back stress, we designed a dedicated setup comprising a heated metallic cantilever and a cold tungsten tip (Figure 2a). The region marked in Figure 2b was observed in detail (Figure 2c–e; Video S4). Because the heating condition is fixed during a given bending-release cycle, the static thermo-elastic pre-load is inherently baselined. Once the convection-like motion began, interfacial deposition progressively deflected the cantilever further, reflecting the accumulation of an incremental net contact force. This force buildup continued until a sudden elastic spring-back occurred (Figure 2e), perfectly synchronized with the plastic collapse of the column. This near-instantaneous spring-back under a constant thermal setting confirms that the measured incremental deflection is dominated by the mechanical back stress generated from interfacial atomic insertion, rather than gradual thermal drift. Failure occurred either by buckling instability or near-uniaxial compressive yielding, and this cycle could repeat many times, enabling multiple independent stress measurements (Note S5). The insertion-induced back stress and column strength were extracted from the equivalent diameters at the contact area (D_C) and at the narrowest section (D_L) of the column (Figure 2d).

Back stress and column strength were extracted from the equivalent diameters at the contact area (D_C) and at the narrowest section (D_L) of the column (Figure 2d). Both quantities exhibited the characteristic nanoscale "smaller is stronger" trend (Figure 2f), with strengths reaching 482 MPa for copper and 338 MPa for silver. The maximum measured back stresses, 75 MPa for copper and 131 MPa for silver, are comparable to those generated in electromigration [21] and thermomigration [1] of metallic interconnects. In practice, column yielding or buckling limits any further rise in interfacial stress [10]. Nevertheless,

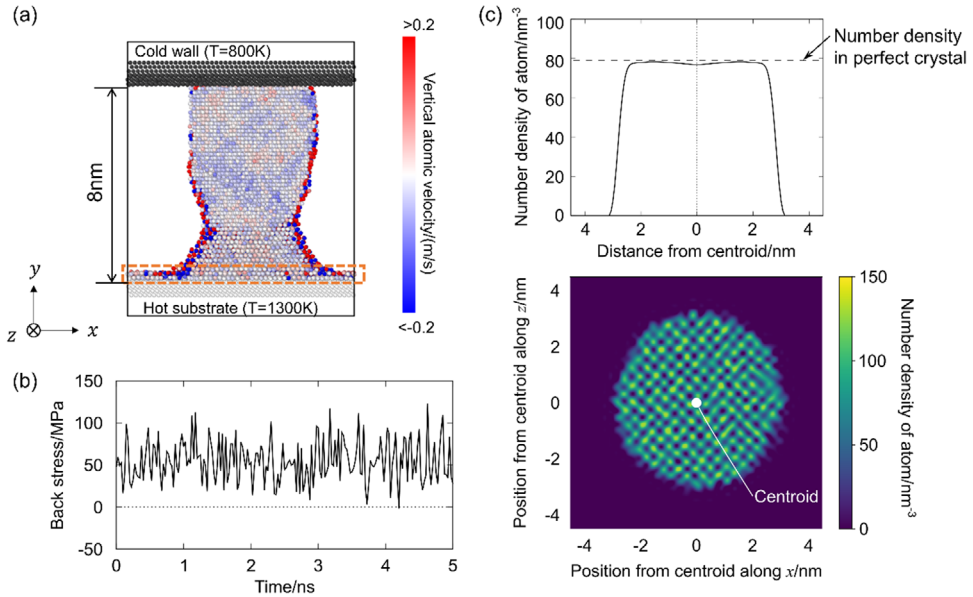

FIGURE 3 | MD simulation results. (a) Cross-section view of the atomic structure and atom velocity in Cu column at 2 ns after reaching steady state. The color indicates the average velocity of atoms in the vertical direction (y-axis direction) for 1 ns. (b) Measured contact back-stress during MD simulation at the steady state. (c) Radial distribution of the number density of atoms at the interface (upper) and 2D interfacial number density distribution (lower) at 5 ns. Note that the left half side of the upper figure is a reversed plot of the right side for the eye guide.

these unusually high stresses, arising from thermo-mechanical coupling under extreme ∇T, are sufficient to power solid-state nano-actuators or "nano-engines."

From the measured back stress, we estimated the minimum temperature gradient using the following equation [1]:

$$\Omega\Delta\sigma = Q(\Delta \ln T) \quad (1)$$

where Q is the heat of transport (0.17 eV for copper [24]), Ω is the atomic volume of copper (1.18×10^{-29} m^3), and $\Delta\sigma$ is the back stress difference. Taking $\Delta\sigma = 75$ MPa and a hot-end temperature of 400°C, the minimum ΔT required is ~42°C. For the longest copper column studied (115 nm), this corresponds to a longitudinal temperature gradient of $\sim 10^8$ K m^{-1}—consistent with our FEM simulations (Figure S8).

2.3 | Molecular Dynamics Simulation

To systematically accelerate atomic-scale diffusive processes and capture steady-state mass transport within the inherently limited timescale accessible to MD simulations, we employed elevated absolute temperatures (hot substrate, 1300 K; cold wall, 800 K) and a larger temperature gradient (6.2×10^{10} K m^{-1}) than those used in the TEM experiments (see Figure 3a and Methods). This computational setup was adopted to reveal the coupled thermo-mechanical transport pathway at the atomic scale, rather than to quantitatively reproduce the exact thermal conditions of the in situ TEM experiments at 400°C (673 K).

To directly examine the upward mass transport, we traced all atoms that moved upward by more than 2 nm and reached the cold end during the 80 ns MD simulation. Their trajectories are shown in Figure S11 and Video S6. These trajectories directly show that atoms migrate from the hot substrate to the cold end along the surface and are subsequently incorporated into the interior of the column through the interface between the column and the cold tip, thereby providing direct atomistic evidence for the proposed convection-like transport pathway.

A possible concern is that the elevated MD temperature (1300 K) could induce extensive surface pre-melting and thereby artificially enhance the upward transport. To examine this possibility, we analyzed the average displacement of surface atoms over a time interval of 0.1 ns in the simulation (Figure S12). Over most of the Cu column surface, the average atomic displacement is approximately 0.15 nm, which is smaller than the nearest-neighbor distance in fcc Cu (0.256 nm), whereas the largest displacement (~0.32 nm) is confined to a very narrow region immediately adjacent to the hot substrate. These results indicate that extensive surface pre-melting does not occur in the present MD simulation and, if present at all, is limited to the immediate vicinity of the hot substrate.

We further examined whether the upward transport remains kinetically feasible at the experimental temperature of 400°C (673 K). The mean-squared-displacement analysis of surface atoms at 400°C yields a surface self-diffusion coefficient of 0.21–0.64×10^{-12} m^2 s^{-1} (Figure S13), which is within one order of magnitude of the value extrapolated to 400°C (4.92×10^{-12} m^2 s^{-1}) from the experimentally reported self-diffusion coefficient of the Cu(110) surface [25]. Using $t \sim h^2/D$ with $h \sim 100$ nm, corresponding to the maximum column height in the experimental sample, the time required for atoms to migrate over this distance is estimated to be on the order of 10 ms. This timescale is consistent with the experimental timescale, indicating that the upward surface transport identified by the MD simulations is kinetically feasible at 400°C without invoking surface pre-melting.

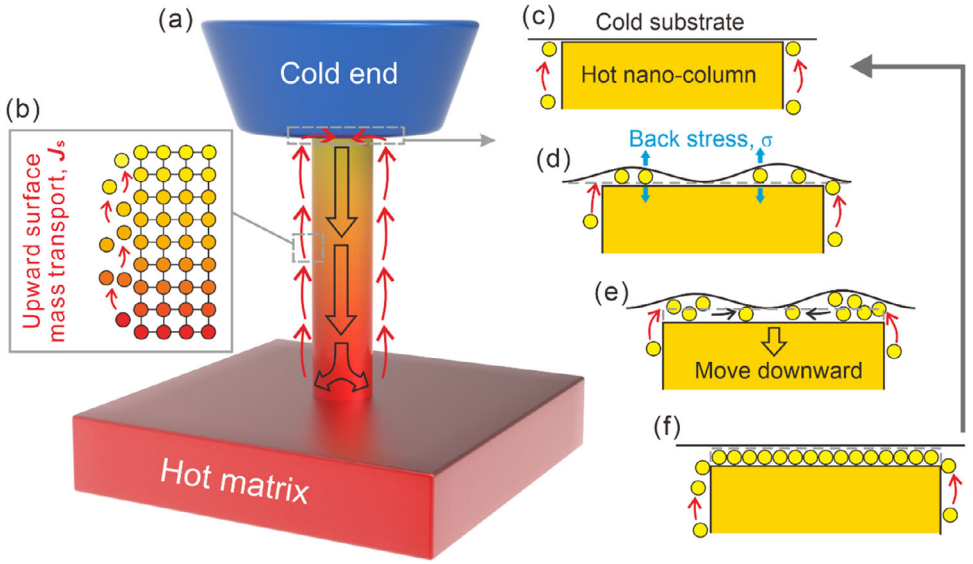

FIGURE 4 | Schematic illustration for the mechanism. The convection-like motion in a nano-column between the hot metal matrix and the cold end (a). The observed mass circulation is enabled by two key processes: the first process is surface mass transport as shown in the left inset (b), and the other one is the insertion and deposition of atoms in the top interface as shown by the right insets (c–f).

After reaching the steady state, the vertical atomic velocities averaged over 1 ns (Figure 3a) clearly reveal a convection-like pattern: upward surface migration of atoms from hot to cold, accompanied by a simultaneous downward translation of the crystalline core (Video S5). The back stress at the cold interface stabilizes at ~50 MPa (Figure 3b), indicating a balance between the surface migration flux and the atomic outflow at the hot end. This value is about an order of magnitude smaller than that predicted from Equation (1) using experimental parameters—likely because classical MD accounts only for phonon-mediated heat of transport, omitting the electron contribution that dominates in conductive metals like Cu. Nevertheless, the simulations qualitatively reproduce the convection-like motion observed in situ under an extreme temperature gradient.

We further examined the interfacial atomic density to understand why incoming atoms preferentially insert into the cold contact rather than nucleating new contact points at the perimeter. The radial and 2D density maps (Figure 3c) show that the central 1 nm region of the contact has a lower atomic density—and thus more free volume—than the surrounding perimeter. This gradient in free volume drives inward atomic flow, steering atoms from the edge toward the central interface, and thereby sustaining the compressive back stress that propels the column.

2.4 | Mechanism of Convection-Like Motion in a Crystalline Solid

The generation of stress and displacement between hot and cold boundaries in our system is akin to a heat engine. Conventional heat engines operate with a working fluid such as steam or air; here, the "working medium" is a crystalline solid. This analogy motivates a closer look at the physical mechanism, which may inspire designs for thermally driven actuators using creeping solids.

The proposed mechanism, illustrated schematically in Figure 4, begins with the establishment of an ultra-high axial temperature gradient (∇T) in a nanoscale column only a few hundred nanometers long. These gradient drives atoms migrating from the hot end toward the cold end, predominantly along the high-mobility surface layer of δ_s. As shown in Figure 4a,b, atoms migrate rapidly along the surface layer under ∇T, while the column's crystalline core remains solid and translates in the opposite direction, toward the hot end, as a rigid body. The driving force for this core translation is the back stress generated at the cold interface. When surface-migrating atoms, propelled by a chemical potential gradient, insert into the confined boundary between the column and the punch tip (Figure 4c,d), they create a "traffic jam" of atomic insertion. This produces a self-regulated compressive stress (σ) that pushes on the weaker element in the contact pair, the slender Cu column, driving it downward (Figure 4d,e). The back stress increases until the column yields or buckles, typically at its hot end.

Surface and interfacial diffusion in this process are coupled to multiple gradients—temperature, stress, and surface conditions—which together define the net atomic flux. A simplified description is:

$$J_S = -\delta_S C_S M_S \nabla (\mu + Q \ln T) \tag{2}$$

where J_s is the atomic flux along the surface, δ_s is the thickness of the high-mobility surface layer, C_s is the atomic concentration in this layer, and $M_s = D_s/k_B T$ is the surface mobility related to the surface diffusivity D_s. The chemical potential $\mu(C_s, \sigma, T)$ includes entropic terms ($k_B T \ln(C_s \Omega)$), with Ω the atomic volume, mechanical contributions ($\Omega \sigma_{nn}$), and curvature- or stress-dependent surface energy terms [26]. Consequently, J_s is linearly sensitive to ∇T, ∇C_s, and $\nabla \sigma$. Divergence of J_s alters C_s and thus the evolving surface profile, creating a feedback loop between $C_s(x,t)$, $\sigma(x,t)$, and $T(x,t)$.

A gradient in surface vacancies or free volume (∇C_s) at the interface is not unusual—similar patterns occur in ZrO_2 nanowires during thermomigration [27]. In our case, MD simulations (Figure 3c) and the schematic in Figure 4c–f indicate that the contact center has more free volume than the perimeter. This geometry draws incoming atoms from the edge inward, sustaining the back stress and driving the downward motion of the core. From a scaling perspective, using literature values for the thermomigration heat ($Q \approx 0.1$ eV), atomic volume ($\Omega \approx 10$ Å^3), and temperature differences ($\Delta \ln T \approx 0.1$), the "solid engine" can generate back stresses on the order of 10^2 MPa—sufficient to drive creep or even displacive plasticity at room temperature. In extreme cases ($\Delta \ln T \approx 1$), σ could approach the gigapascal range.

3 | Conclusion

We have demonstrated a circular, convection-like motion in a nanoscale crystalline solid subjected to an ultra-high axial temperature gradient. In this process, atoms migrate upward along the surface via diffusive thermo-mechanical migration, while the crystalline core returns downward through a back-stress-driven displacive motion, forming a closed-loop flow with a core–shell structure. The mechanism is therefore hybrid in nature: surface diffusion governs the upward migration of atoms along the surface, while bulk displacive motion governs the downward return of the crystalline core. Although thermal convection is well established in fluids, our observations reveal that a similar circulation can occur in nanoscale solids, driven not by gravity or thermal expansion—as in Rayleigh–Bénard convection—but by coupled thermo-mechanical surface mass transport under extreme ∇T.

This phenomenon bears some resemblance to the Kirkendall effect, which also involves rigid-body translation and interfacial vacancy sources/sinks. However, the underlying physics is fundamentally different. In the Kirkendall effect, a chemical-potential-driven lattice-vacancy flux dominates [28], whereas here, the primary driver is the coupled thermo-mechanical surface diffusion under a gigantic temperature gradient, with the self-generated back stress providing the mechanical return.

Viewed through the framework of non-equilibrium thermodynamics, this surface-diffusion-induced motion represents an off-diagonal Onsager coupling: a temperature gradient that primarily drives heat flow (Fourier's law) also induces a mass flux, as surface atoms act as both heat and mass carriers. This is analogous to the thermoelectric effect, where the heat of transport (Q) quantifies the coupling. Such heat-to-mass conversion at the nanoscale suggests a new class of solid-state "heat engines" in which the working medium is a crystalline solid rather than a fluid.

The implications extend beyond fundamental physics. In MEMS and NEMS devices, where structural dimensions range from tens to hundreds of nanometers, even a modest temperature difference of a few kelvins can produce ∇T on the order of 10^7–10^8 K m^{-1}. Under these conditions, surface or interfacial atomic migration can generate back stresses of hundreds of MPa, potentially altering morphology, shifting positions, or compromising structural integrity. Reported consequences include thermomigration-induced nanowire growth [1, 27], internal stress accumulation [21], bending, and fracture or failure of microfabricated components [29–34]. In geometrically confined structures, the coexistence of thermomigration, stress-assisted atom migration, and back stress could give rise to the type of convection-like motion we observed here. Our findings also indicate that the surface passivation, by suppressing surface mass transport, offers an effective strategy to mitigate these effects.

4 | Methods

4.1 | Sample Preparation

High purity aluminum (99.9995%), silver (99.999%), and copper (99.99%) were cut into thin plates with size of 2 mm × 1.5 mm × 0.6 mm via the wire-cutting machine, respectively. Then the plate was mechanically grinded to a thickness of ~0.1 mm using silicon carbide sandpapers from #800 to #2000. One edge of the grinded samples was further thinned to several micrometers by electrochemical polishing. After that, samples were glued on the commercial Hysitron MEMS heater using special epoxy conductive glue, which could hold 500 °C high temperature. Finally, the samples were further fabricated by focused ion beam (FIB, FEI Helios Nanolab 600i) with 30 kV Ga^+ from current of 2.8 nA to 9.7 pA to get ~200-nm pillars as the metal matrix.

4.2 | In Situ TEM Convection Experiments

The in situ convection experiments were carried out with a Hysitron PI95 ECR PicoIndenter holder equipped in JEOL-2100F field emission gun transmission electron microscope (FEG-TEM) and a Hysitron PI95 H1H PicoIndenter holder coupled in Hitachi H-9500 environmental transmission electron microscope (E-TEM). The MEMS platform (Figure S1) ensures precise thermal stability using two electrically independent platinum (Pt) coils for Joule heating and real-time sensing. A closed-loop feedback system dynamically modulates input power, strictly restricting temperature fluctuations to <0.5°C. Combined with the substrate's large thermal mass, this active regulation enables the fabricated cantilevers to function as a stable thermal reservoir throughout the entire observation. To trigger the convection-like motions, samples were heated to elevated temperatures (400°C for Cu and Al, and 300°C for Ag) with a rate of 30°C/min. Subsequently, the piezo-driven cold W tip was carefully manipulated to contact the hot fresh metal matrix, followed by pulling backward with speed of a few nanometers per second and then holding a constant spacing. In such way, the convection-like motion of crystalline copper, silver, and aluminum could be formed between the cold tip and hot matrix. The whole process was in situ recorded by the Gatan Orius 832 CCD camera at rate of 10 frames per second.

4.3 | In Situ TEM Cantilever Bending Experiments

The silver and copper cantilevers were fabricated by FIB using previous foil samples attached on MEMS heaters. The voltage of gallium ion beam was 30 kV with processing current from

2.8 nA to 9.7 pA. The size of fabricated cantilevers was ~4 μm (length) × ~320 nm (height) × ~280 nm (width). The in situ bending experiments were performed with the Hysitron PI95 PicoIndenter ECR holder equipped with a MEMS heater in JEOL-2100F FEG-TEM. Both goal temperature and heating rate were identical to those previously discussed in the experimental setup, and the convection-like motion was locally triggered at the head of cantilevers using the same methods as described before. The process was recorded by the Gatan Orius 832 CCD camera with the rate of 10 frames per second.

4.4 | Molecular Dynamics Simulations

Molecular dynamics simulations with temperature gradient were performed using the Large-scale Atomic/Molecular Massively Parallel Simulator (LAMMPS) package [35]. A Cu column model of 6 nm diameter and 8 nm height bounded by a hot Cu substrate and a cold wall was used. The embedded atom method (EAM) potential for Cu [36] was employed for the interatomic interaction for Cu atoms. To model the low-wettability between the Cu column and the cold wall, we used a two-body interaction between the Cu atom and the atom in the cold wall, $\phi(r) = \varepsilon[(r_0/r)^p\text{-}(r_0/r)^q]$ where $\varepsilon = 0.09$ eV, $r_0 = 0.226$ nm, $p = 8.55$, and $q = 4.49$, respectively. The model was first annealed at 727°C (1000 K) for 1 ns. Then, the cold wall and the substrate were maintained at temperatures of 527°C (800 K) and 1027°C (1300 K), respectively. Thus, the temperature gradient was 6.2×10^{10} K/m. The top four atomic layers in the cold wall and the bottom four layers in the Cu substrate were fixed to maintain the positions of the cold wall and the substrate. The reaction force acting on the fixed region in the cold wall was measured to estimate the back-stress. A 2D histogram of atom distribution in the top layer of Cu column was used to obtain the interfacial atomic density distribution. The bin width was set to 0.2 nm. The number density was determined as an average of 100 snapshots with an interval of 10^5 MD steps (100 ps).

4.5 | DFT Calculations on Doping Cu Atoms in WO_3 and W Solid Solutions

The DFT simulations were performed using the VASP code [37] with projector-augmented wave (PAW) pseudopotentials [38] and Perdew–Burke–Ernzerhof (PBE) gradient-corrected functional [39]. A cutoff energy of 500 eV for plane waves was used. A 4 × 4 × 4 k-point mesh was employed to sample the Brillouin zone. The pristine WO_3 with two different phases in supercells, i.e., the cubic phase and the monoclinic phase. Each model has 32 atoms in total. The lattice constants and atomic positions are relaxed to reach the minimum of external pressure and atomic forces.

4.6 | FEM Thermal Simulations

To quantitatively estimate the temperature distribution and temperature gradient along the copper column, we performed the FEM simulation via the COMSOL software. The model was simplified as a 120-nm-long copper nano-column with a cross-sectional diameter of 55 nm (average equivalent diameter for the nano-column in Figure 1), sandwiched by a cold tungsten tip at room temperature and the hot copper substrate at 400°C. Notice the surface of the tungsten tip was set as 5-nm-thickness tungsten trioxide, in line with the experimental/reported situation [40]. The constructed geometry and boundary conditions of the modeling are shown in Figure S8a,b.

We applied the size-dependent thermal conductivity values reported in the literature for the temperature simulation. The thermal conductivity of the copper column was estimated as 140 W/m·K, on the basis of the calculation of copper nanowires with similar sizes reported by Stojanovic et al. [41]. Regarding the thermal conductivity of the tungsten trioxide with a thickness of 5 nm, we found no reported values with a similar size but rather the value of a tungsten trioxide thin film with a thickness of 100 nanometers [42]. As such, the reported thermal conductivity of a 100-nm-thickness tungsten trioxide thin film, 1.63 W/m·K, was employed for the FEM simulation.

Author Contributions

Z.S. and J.L. designed and supervised the project. Y.Y., Z.N., and X.W. performed the in situ TEM experiments. Y.Y. and D.X. carried out the in situ TEM data analysis. S.S. performed the MD simulations under the supervision of S.O. Z.N. performed the FEM simulations. S.S. conducted DFT simulations under the supervision of W.Z. E.M. contributed to the interpretations of the observations. Y.Y., D.X. and S.S. wrote the paper with input from J.L., E.M., S.O. and Z.S. All authors contributed to discussions of the results.

Acknowledgements

The authors acknowledge the supports from Natural Science Foundation of China (52371122, 52522103), Shaanxi Province Foundation for Distinguished Young Scholars (2024JC-JCQN-47). Y.Y acknowledges the support by the Natural Science Foundation of Shandong Province (ZR2024QE239). S.S. and S.O. acknowledge the large-scale computer systems at the D3 Center, The University of Osaka, the Large-scale parallel computing server at the Center for Computational Materials Science, Institute for Materials Research, Tohoku University, Research Center for Computational Science, Okazaki, Japan (Project: 25-IMS-C503), and supercomputer Fugaku provided by the RIKEN Center for Computational Science (hp250229 and hp250227). S.O. acknowledges the support by the JSPS KAKENHI (JP17H01238, JP21K18675, JP23K20037) and MEXT Programs (JPMXP1122684766, JPMXP1020230325, JPMXP1020230327). S.S. acknowledges the support by the JSPS KAKENHI (JP21K14042, 22H05283, 24K17170, 24H00994). W.Z. and E.M. acknowledges XJTU for supporting their work at CAID.

Conflicts of Interest

The authors declare no conflicts of interest.

Data Availability Statement

The data that support the findings of this study are available from the corresponding author upon reasonable request.

References

1. D. G. Xie, Z. Y. Nie, S. Shinzato, et al., "Controlled Growth of Single-Crystalline Metal Nanowires via Thermomigration Across a Nanoscale Junction," *Nature Communications* 10, no. 1 (2019): 4478, https://doi.org/10.1038/s41467-019-12416-x.

2. S. Liang, H. Jiang, R. Zhou, et al., "Study on Thermomigration-Induced Void Formation in Advanced Copper Interconnects," *IEEE Transactions*

on Components, Packaging and Manufacturing Technology 15, no. 8 (2025): 1692–1697, https://doi.org/10.1109/TCPMT.2025.3530423.

3. J. Sun, L. He, Y. C. Lo, et al., "Liquid-Like Pseudoelasticity of Sub-10-nm Crystalline Silver Particles," *Nature Materials* 13, no. 11 (2014): 1007–1012, https://doi.org/10.1038/nmat4105.

4. S. Zheng, X. Wang, S. Tan, et al., "Atomistic Processes of Diffusion-Induced Unusual Compression Fracture in Metallic Nanocrystals," *Materials Research Letters* 10, no. 12 (2022): 805–812, https://doi.org/10.1080/21663831.2022.2108349.

5. S. Azadehranjbar, R. Ding, I. M. Padilla Espinosa, et al., "Size-Dependent Role of Surfaces in the Deformation of Platinum Nanoparticles," *ACS Nano* 17, no. 9 (2023): 8133–8140, https://doi.org/10.1021/acsnano.2c11457.

6. L. He, S. Yang, L. Shangguan, et al., "Surface-Governed Deformation Mechanisms in Sub-20-nm Metallic Crystals Stimulated by Electrical Loading," *Materials Today Nano* 22 (2023): 100310, https://doi.org/10.1016/j.mtnano.2023.100310.

7. J. Jiang, S. Chu, Y. Zhang, et al., "Crystal Plane Orientation-Dependent Surface Atom Diffusion in Sub-10-nm Au Nanocrystals," *Science Advances* 10, no. 21 (2024): eadn5946, https://doi.org/10.1126/sciadv.adn5946.

8. C. E. Carlton, F. Zorro, M. J. Caturla, et al., "Nanocompression of 20 nm Silver Nanoparticles: In situ Aberration-Corrected TEM and Atomistic Simulations," *Small* 21, no. 4 (2025): 2405292, https://doi.org/10.1002/smll.202405292.

9. Y. Chen, Z. Wang, X. Li, et al., "Li Metal Deposition and Stripping in A Solid-State Battery via Coble Creep," *Nature* 578, no. 7794 (2020): 251–255, https://doi.org/10.1038/s41586-020-1972-y.

10. L. Zhang, T. Yang, C. Du, et al., "Lithium Whisker Growth and Stress Generation in an In Situ Atomic Force Microscope-Environmental Transmission Electron Microscope Set-up," *Nature Nanotechnology* 15, (2020): 94–98, https://doi.org/10.1038/s41565-019-0604-x.

11. Y. Hu, S. Li, and H. Bao, "First-principles Based Analysis of Thermal Transport in Metallic Nanostructures: Size Effect and Wiedemann-Franz Law," *Physical Review B* 103, no. 10 (2021): 104301, https://doi.org/10.1103/PhysRevB.103.104301.

12. A. Wang and H. Bao, "Size-Dependent Thermal Transport Properties of Advanced Metallic Nanowire Interconnects," *Applied Physics Letters* 124, no. 21 (2024): 212202, https://doi.org/10.1063/5.0206103.

13. B. Amelia, R. Riccardo, E. R. Hernández, et al., "Subnanometer Motion of Cargoes Driven by Thermal Gradients along Carbon Nanotubes," *Science* 320, no. 5877 (2008): 775–778.

14. Z. Dong, "*Fundamentals of Crystallography, Powder X-ray Diffraction, and Transmission Electron Microscopy for Materials Scientists*," CRC Press, https://doi.org/10.1201/9780429351662.

15. A. Kryshtal, S. Bogatyrenko, and O. Khshanovska, "Direct Imaging of Surface Melting on a Single Sn Nanoparticle," *Nano Letters* 23, no. 14 (2023): 6354–6359, https://doi.org/10.1021/acs.nanolett.3c00943.

16. H. Fang, Y. Pan, B. Wu, C. Lu, W. Ouyang, and Z. Liu, "Diffusion-Mediated Superelongation in Metal Nanorods," *Physical Review Letters* 132, no. 25 (2024): 256201, https://doi.org/10.1103/PhysRevLett.132.256201.

17. Y. Yang, L. Gu, T. Mao, et al., "In Situ Observation of the Layer-by-Layer Melting of the Au(200) Surface in Nanoporous Gold," *The Journal of Physical Chemistry C* 129, no. 51 (2025): 22454–22462, https://doi.org/10.1021/acs.jpcc.5c06128.

18. X. Wang, S. Zheng, S. Shinzato, et al., "Atomistic Processes of Surface-diffusion-induced Abnormal Softening in Nanoscale Metallic Crystals," *Nature Communications* 12, no. 1 (2021): 5237, https://doi.org/10.1038/s41467-021-25542-2.

19. W. Li, J. M. Rieser, A. J. Liu, D. J. Durian, and J. Li, "Deformation-driven Diffusion and Plastic Flow in Amorphous Granular Pillars," *Physical Review E* 91, no. 6 (2015): 062212, https://doi.org/10.1103/PhysRevE.91.062212.

20. D. Lohse and O. Shishkina, "Ultimate Rayleigh-Bénard Turbulence," *Review of Modern Physics* 96, no. 3 (2024): 035001, https://doi.org/10.1103/RevModPhys.96.035001.

21. I. A. Blech, "Diffusional Back Flows during Electromigration," *Acta Materialia* 46, no. 11 (1998): 3717–3723, https://doi.org/10.1016/S1359-6454(97)00446-1.

22. Z. Tafferner, D. Bušek, and A. Géczy, "Electromigration Behaviour of Solder Joints under High Current Load: A Review," *Materials Today Electronics* 16, (2026): 100211, https://doi.org/10.1016/j.mtelec.2026.100211.

23. P. Cheng, L. Mao, W. Shen, et al., "Electromigration Failures in Integrated Circuits: A Review of Physics-Based Models and Analytical Methods," *Electronics* 14, no. 15 (2025): 3151, https://doi.org/10.3390/electronics14153151.

24. C. M. Tan and A. Roy, "Investigation of the Effect of Temperature and Stress Gradients on Accelerated EM Test for Cu Narrow Interconnects," *Thin Solid Films* 504, no. 1 (2006): 288–293, https://doi.org/10.1016/j.tsf.2005.09.101.

25. D. B. Butrymowicz, J. R. Manning, and M. E. Read, "Diffusion in Copper and Copper Alloys. Part I. Volume and Surface Self-Diffusion in Copper," *Journal of Physical and Chemical Reference Data* 2, no. 3 (1973): 643–656, https://doi.org/10.1063/1.3253129.

26. Q.-J. Li, B. Xu, S. Hara, J. Li, and E. Ma, "Sample-size-dependent Surface Dislocation Nucleation in Nanoscale Crystals," *Acta Materialia* 145 (2018): 19–29, https://doi.org/10.1016/j.actamat.2017.11.048.

27. K. S. N. Vikrant, R. L. Grosso, L. Feng, et al., "Ultrahigh Temperature in Situ Transmission Electron Microscopy Based Bicrystal Coble Creep in Zirconia I: Nanowire Growth and Interfacial Diffusivity," *Acta Materialia* 199 (2020): 530–541, https://doi.org/10.1016/j.actamat.2020.08.069.

28. E. O. Kirkendall, "Diffusion of Zinc in Alpha Brass," *Transactions AIME* 147, (1942): 104–109.

29. P. Liu, S. Cong, S. Wang, et al., "Thermomigration-Induced Failure in Ball Grid Array Solder Joint under High Current Stressing," *Journal of Materials Science* 58, no. 26 (2023): 10753–10763, https://doi.org/10.1007/s10853-023-08678-y.

30. N. T. Anthony, "Thermal Gradient Induced Failure Mechanisms in High Power Semiconductor Devices Under Operational Stress Conditions," *International Journal of Computer Applications Technology and Research* 14, no. 4 (2025): 97–113, https://doi.org/10.7753/IJCATR1404.1008.

31. Y. Ding, O. V. Pedreira, M. Lofrano, et al., "Thermomigration-Induced Void Formation in Cu-Interconnects - Assessment of Main Physical Parameters," *2023 IEEE International Reliability Physics Symposium (IRPS)* (2023): 1–7, https://doi.org/10.1109/IRPS48203.2023.10117870.

32. O. V. Pedreira, Y. Ding, D. Coenen, et al., "De-Coupling Thermo-Migration from Electromigration Using a Dedicated Test Structure," *2024 IEEE International Reliability Physics Symposium (IRPS)* (2024): 1–5, https://doi.org/10.1109/IRPS48228.2024.10529380.

33. Y. Ding, O. V. Pedreira, D. Coenen, et al., "Analytical Model for Cu Interconnect Lifetimes Under Combined Thermomigration and Electromigration Stress," *IEEE Transactions on Device and Materials Reliability* 25, no. 4 (2025): 983–993, https://doi.org/10.1109/TDMR.2025.3629672.

34. Y. Ding, O. V. Pedreira, M. Lofrano, et al., "Cu Interconnect Lifetime Estimation in the Presence of Thermal Gradients," *Journal of Applied Physics* 137, no. 7 (2025): 075106, https://doi.org/10.1063/5.0245489.

35. S. Plimpton, "Fast Parallel Algorithms for Short-Range Molecular Dynamics," *Journal of Computational Physics* 117, no. 1 (1995): 1–19, https://doi.org/10.1006/jcph.1995.1039.

36. F. Fischer, G. Schmitz, and S. M. Eich, "A Systematic Study of Grain Boundary Segregation and Grain Boundary Formation Energy Using a New Copper–nickel Embedded-atom Potential," *Acta Materialia* 176 (2019): 220–231, https://doi.org/10.1016/j.actamat.2019.06.027.

37. G. Kresse and J. Furthmüller, "Efficient Iterative Schemes for Ab Initio Total-energy Calculations Using a Plane-wave Basis Set," *Physical Review B* 54, no. 16 (1996): 11169–11186, https://doi.org/10.1103/PhysRevB.54.11169.

38. P. E. Blöchl, "Projector Augmented-wave Method," *Physical Review B* 50, no. 24 (1994): 17953–17979, https://doi.org/10.1103/PhysRevB.50.17953.

39. J. P. Perdew, K. Burke, and M. Ernzerhof, "Generalized Gradient Approximation Made Simple," *Physical Review Letters* 77, no. 18 (1996): 3865–3868, https://doi.org/10.1103/PhysRevLett.77.3865.

40. E. Lassner and W. D. Schubert, *Tungsten: Properties, Chemistry, Technology of the Elements, Alloys, and Chemical Compounds*, (Springer, 1999), https://doi.org/10.1007/978-1-4615-4907-9.

41. N. Stojanovic, D. H. S. Maithripala, J. M. Berg, and M. Holtz, "Thermal Conductivity in Metallic Nanostructures at High Temperature: Electrons, Phonons, and the Wiedemann-Franz Law," *Physical Review B* 82, no. 7 (2010): 82, https://doi.org/10.1103/PhysRevB.82.075418.

42. H. T. Wang, Y. B. Xu, M. Goto, et al., "Thermal Conductivity Measurement of Tungsten Oxide Nanoscale Thin Films," *Materials Transcations* 47, no. 8 (2006): 1894–1897, https://doi.org/10.2320/matertrans.47.1894.

Supporting Information

Additional supporting information can be found online in the Supporting Information section.

Supporting File 1: smll73634-sup-0001-SuppMat.docx.

Supporting File 2: smll73634-sup-0002-VideoS1.mp4.

Supporting File 3: smll73634-sup-0003-VideoS2.mp4.

Supporting File 4: smll73634-sup-0004-VideoS3.mp4.

Supporting File 5: smll73634-sup-0005-VideoS4.mp4.

Supporting File 6: smll73634-sup-0006-VideoS5.mp4.

Supporting File 7: smll73634-sup-0007-VideoS6.mp4.